Frontiers of Optoelectronics (2023) 16:5
https://doi.org/10.1007/s12200-023-00060-9

Frontiers of Optoelectronics

RESEARCH ARTICLE

Design and modeling of high-performance mid-wave infrared InAsSb-based nBn photodetector using barrier band engineering approaches

Maryam Shaveisi[1] · Peiman Aliparast[1]

Received: 5 December 2022 / Accepted: 17 February 2023
© The Author(s) 2023

Abstract
We report a new nBn photodetector (nBn-PD) design based on the InAlSb/AlSb/InAlSb/InAsSb material systems for mid-wavelength infrared (MWIR) applications. In this structure, delta-doped compositionally graded barrier (δ-DCGB) layers are suggested, the advantage of which is creation of a near zero valence band offset in nBn photodetectors. The design of the δ-DCGB nBn-PD device includes a 3 μm absorber layer (n-$InAs_{0.81}Sb_{0.19}$), a unipolar barrier layer (AlSb), and 0.2 μm contact layer (n-$InAs_{0.81}Sb_{0.19}$) as well as a 0.116 μm linear grading region (InAlSb) from the contact to the barrier layer and also from the barrier to the absorber layer. The analysis includes various dark current contributions, such as the Shockley–Read–Hall (SRH), trap-assisted tunneling (TAT), Auger, and Radiative recombination mechanisms, to acquire more precise results. Consequently, we show that the method used in the nBn device design leads to diffusion-limited dark current so that the dark current density is 2.596×10^{-8} A/cm^2 at 150 K and a bias voltage of − 0.2 V. The proposed nBn detector exhibits a 50% cutoff wavelength of more than 5 μm, the peak current responsivity is 1.6 A/W at a wavelength of 4.5 μm and a − 0.2 V bias with 0.05 W/cm^2 backside illumination without anti-reflective coating. The maximum quantum efficiency at 4.5 μm is about 48.6%, and peak specific detectivity (D*) is of 3.37×10^{10} cm·Hz$^{1/2}$/W. Next, to solve the reflection concern in this nBn devices, we use a BaF_2 anti-reflection coating layer due to its high transmittance in the MWIR window. It leads to an increase of almost 100% in the optical response metrics, such as the current responsivity, quantum efficiency, and detectivity, compared to the optical response without an anti-reflection coating layer.

Keywords Mid-wave infrared detectors · III-V compound semiconductors · Grading material systems · nBn architecture

1 Introduction

The InAsSb infrared detectors show the highest performances among all infrared detectors due to their excellent optical and electrical properties, which is the reason why the use of the InAsSb material in the semiconductor industry has a long history [1]. The InAsSb material has the lowest band gap energy among group III-V semiconductors. It can be used as an active region material for designing mid-wavelength infrared (MWIR) and long-wavelength infrared (LWIR) optical detectors [2, 3]. However, the limitations of conventional PN or PIN photodiodes operating under high operating temperature conditions indicate that the dark current is mainly generated by Shockley–Read–Hall (SRH) generation-recombination (GR), Auger recombination, band-to-band tunneling (BTBT) and trap-assisted tunneling (TAT) processes [4]. Also, with avalanche photodiodes (APDs) using the impact ionization process, it is possible to achieve higher sensitivity than with conventional photodetectors. However, these detectors also show a high dark current due to the carrier recombination effect [5]. Previous studies suggest that a wide band gap material used as a barrier between the contact layer and the absorber layer can expand the operating temperature, reducing the dark current caused by the majority of carriers [6]. Among the reported barrier detectors, the nBn photodetectors have received the most attention in commercialization [7–13]. In 2006, Maimon and Wicks introduced nBn detectors and published one of the most influential works [14]. This work states that the performance of nBn photodetector is controlled by a barrier

✉ Maryam Shaveisi
M_Shaveisi@ari.ac.ir

[1] Aerospace Research Institute (Ministry of Science, Research and Technology), Tehran 1465774111, Iran

Published online: 06 April 2023

layer. The barrier layer material is a semiconductor with a large band gap energy, located between the two contacts and the narrow band gap absorber layer. Majority carriers are blocked, but there is no barrier for minority carriers to pass. These unipolar barriers are used to suppress the two main dark current mechanisms, GR dark current and surface leakage current [15]. First infrared nBn detectors were built by the growth of the InAs absorber layer on the InAs substrate and also the growth of the $InAs_{0.91}Sb_{0.09}$ alloy on the lattice-matched GaSb substrate [14]. These devices have cutoff wavelengths of 3.2 and 4 µm, respectively. Like InSb infrared photodetectors, they do not cover the whole mid-infrared wavelength range (3–5 µm) but can operate at higher temperatures than InSb detectors [16]. Ting et al. have modeled the standard InAsSb-based nBn photodetector described by Maimon and Wicks. They have investigated the effects of doping in the contact and absorber layers and minority carrier lifetimes which affect the dark current of the proposed nBn structure. Their study showed that the dark current can be reduced by proper design, and the maximum quantum efficiency can be obtained [17]. For achieving optimal performance in InAsSb-based nBn structures, the barrier layer must be designed to create the maximum conduction band offset (CBO) and the minimum valence band offset (VBO). However, finding a material with a large band gap, a large CBO, and a slight VBO is complicated. Previous studies have proposed several band engineering methods to compensate for the valence band discontinuity problem in nBn structures. Among them, the most common ones are the simultaneous grading doping concentration and material composition, and barrier layer methods based on semiconductor superlattice [12, 13, 18, 19]. Recently, Deng et al. have reported a new InAsSb-based nBn detector with $AlAs_{0.08}Sb_{0.92}$/AlSb compound barrier layer [20]. By designing a 100 nm thick $AlAs_{0.08}Sb_{0.92}$/AlSb compound barrier layer, they were able to reduce the VBO in nBn detectors. The simulation results have confirmed that the dark current caused by GR processes, tunneling, and surface leakage currents were effectively suppressed. In addition, the operating temperature was raised to about 205 K. In another study, Deng et al. have suggested an MWIR photodetector based on pCBn architecture [21]. They have utilized short-period $AlAs_{0.08}Sb_{0.92}$/AlSb (4/1.5 mono-layers (MLs)) superlattices with a thickness of 150 nm as the barrier. This compound barrier layer has created a lower VBO and higher CBO than is achieved by the $AlAs_{0.08}Sb_{0.92}$ barrier. The simulation results have shown that the device has good high-temperature performance, and the main mechanisms of dark current can be relatively suppressed.

In this study, we introduce a new infrared photodetector device called a delta-doped compositionally graded barrier nBn photodetector (δ-DCGB nBn-PD) to minimize the VBO in $InAs_{0.81}Sb_{0.19}$ based nBn structures while maximizing the CBO. The AlSb layer, a typical barrier, has a VBO for the InAsSb layer with a Sb composition above 15% [22]. This method, which is developed based on δ-doped layers in the vicinity of the barrier layer, is used together with a compositionally graded barrier layer. This method has been successfully applied to InGaAs and HgCdTe unipolar detectors [23, 24], but so far it has not been implemented for InAsSb nBn detectors. The proposed method used to reduce the VBO in this structure is more convenient than previously presented methods, and it can be fabricated by using the molecular beam epitaxy (MBE) technique. A benefit of this approach is that it does not require simultaneous grading of n- and p-type doping profiles. Another critical issue is that in focal plane arrays (FPAs), which is usually irradiated from the back, infrared light is absorbed through the substrate on which the detector array is grown. Besides, conventional detectors have significant reflection losses at the air/semiconductor interface, so an anti-reflection coating must be included to reduce these losses. Unfortunately, it is complicated to engineer an anti-reflection coating that works effectively over the entire spectral range with very low reflection intensity. In this design, we propose the use of BaF_2. It gives no external reflection and has significant transmission ability in the MWIR range. Based on the simulation results, it can be said that this approach significantly increases the responsivity and quantum efficiency of the nBn detector.

2 Simulation approach and IR-detector design

As seen in Fig. 1, the proposed nBn photodetector is designed based on the compositionally graded barrier (CGB) method that employs the InAlSb material system. The main layers of the proposed device, which has a 30 µm × 30 µm area, can be grown on the GaSb:Te(100) substrate. The epilayers of the structure start with a buffer layer of 2 µm InGaSb, with n-type doping of 1×10^{15} cm^{-3}. It is used to provide better lattice matching between the layers. Then an n-type $InAs_{0.81}Sb_{0.19}$ absorber layer with a thickness of 3 µm is placed, with a doping level of 3×10^{15} cm^{-3}. On top of the absorber layer, a 0.116 µm grading layer of InAlSb should be grown. Then, the n-type AlSb barrier layer with a thickness of 0.2 µm and doping of 1×10^{16} cm^{-3} is positioned. The thickness of the barrier layer is sufficient to prevent electron tunneling between the contact layer and the absorber layer. Similarly, another InAlSb layer with a thickness of 0.116 µm is placed as the top-grading layer. In the end, the $InAs_{0.81}Sb_{0.19}$ contact layer is also designed with a thickness of 0.1 µm and doping density of 1×10^{16} cm^{-3}.

The design parameters of the device discussed in this paper are listed in Table 1. In the simulation, the use of a detailed material model is required, and some important

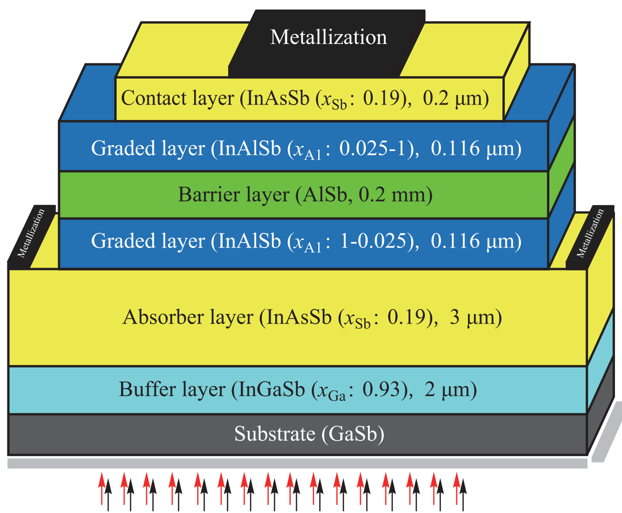

Fig. 1 Schematic of the proposed InAsSb nBn photodetector structure

Table 1 Design parameters of the proposed nBn photodetector used in the simulation

Layer	nBn structure
Contact	
Material	InAsSb (x_{Sb}: 0.19)
Doping/cm^{-3}	n: 3×10^{15}
Thickness/μm	0.2
Grading	
Material	InAlSb (x_{Al}: 0.025–1)
Doping/cm^{-3}	n: 1×10^{16}
Thickness/μm	0.116
δ-doping	
Material	InAlSb (x_{Al}: 0.025,1)
Doping/cm^{-3}	n: 7×10^{15}, p: 1×10^{17}
Thickness/nm	2
Barrier	
Material	AlSb
Doping/cm^{-3}	Undoped
Thickness/μm	0.2
Absorber	
Material	InAsSb (x_{Sb}: 0.19)
Doping/cm^{-3}	n: 3×10^{15}
Thickness/μm	3
Buffer	
Material	InGaSb (x_{Ga}: 0.93)
Doping/cm^{-3}	n: 3×10^{17}
Thickness/μm	2
Substrate	
Material	GaSb
Doping/cm^{-3}	n: 5×10^{17}
Thickness/μm	10

parameters are collected from literatures [25–28]. The structures of the proposed detectors are modeled using the Atlas module in the Silvaco device simulator. This tool uses a set of material properties to characterize the III-V semiconductors, such as energy band gap, electron affinity, dielectric constant, electron and hole mobility, conduction and valance band states densities, and others. In the simulation, we set the parameter values based on the equations and data reported by the Ioffe physical-technical institute (see the website of ioffe.ru). We use the Blaze tool to plot the band structure, which is interfaced with the Atlas module. In addition, the optical response of the device is analyzed using the Luminous tool in the Atlas simulator. Luminous is an advanced device simulator capable of modeling light absorption and generation in III-V semiconductor devices. The absorption coefficient α is dependent on wavelength (or photon energy E), temperature T and mole fraction x of absorber layer, and can be computed for the InAsSb-based detector using Eqs. (1) and (2). Further considerations about the optical properties can be found in the literature reported by D'souza et al. [29]. If the photon energy is less than the energy band gap:

$$\alpha(E,x,T) = 948.23 \times \mathrm{e}^{170(E-E_0)}\,,\quad E_0 = E_{\mathrm{g}} + 0.001\,. \tag{1}$$

While if the photon energy is greater than the energy band gap:

$$\alpha(E,x,T) = \frac{\left[K(E-E_{\mathrm{g}}-c)\sqrt{(E-E_{\mathrm{g}}-c)^2-c^2}\right]}{E} + 800\,,\quad K = 10000 + 20000E_{\mathrm{g}}\,,\quad c = 0.1 + 0.5E_{\mathrm{g}}\,. \tag{2}$$

The following equation is used to model the energy band gap E_{g} of the InAsSb compound, which is dependent on temperature (T, measured in K) and mole fraction of Sb (x_{Sb}) [30]:

$$E_{\mathrm{g}}(x_{\mathrm{Sb}},T) = 0.411 - \frac{3.4\times10^{-4}T^2}{210+T} - 0.876x_{\mathrm{Sb}} + 0.70x_{\mathrm{Sb}}^2 + 3.4\times10^{-4}x_{\mathrm{Sb}}T(1-x_{\mathrm{Sb}})\,. \tag{3}$$

The energy band gap of the InAlSb compound is modeled based on Eq. (4) [31]:

$$E_{\mathrm{g}}(x_{\mathrm{Al}},T) = 0.235 - \frac{3.2\times10^{-4}T^2}{T+170} + 1.721x_{\mathrm{Al}} \ldots - \left(\frac{4.2}{T+140} - \frac{3.2}{T+170}\right)10^{-4}T^2x_{\mathrm{Al}} + 0.43x_{\mathrm{Al}}^2\,. \tag{4}$$

Solving Poisson's equation and using the drift–diffusion model, which includes electrical and optical characteristics, makes it possible to model the device accurately in Silvaco software. For more accurate modeling of nBn detector performance, models for SRH, Auger, radiative, and tunneling recombination are also considered. In our simulations, the recombination parameters, such as the SRH carrier lifetime (τ_n and τ_p), the Auger recombination coefficient, the radiative recombination coefficient, and the activation parameters of donor traps, are modeled using the data given in Table 2 [32, 33].

Also, Refs. [27, 30, 32] provide more information about proposed recombination models, especially the tunneling models. Here, the compositionally graded InAlSb barrier layer is obtained by gradually changing the mole fraction of Al in the InAlSb to grade from a narrow band gap material to a wideband gap material while maintaining the lattice constant. As seen in Fig. 2a, b the band structure without band engineering is contrary to that of the ideal design. In addition to the conduction band barrier, there is also a barrier for minority carriers in the valence band. A band engineering method is presented in this study to remove the barrier of minority carriers. In this method, n and p δ-doped nanolayers are placed on both sides of the graded barrier layers, with p-type δ-doped nanolayers at the interface with wide band gap material, and p-type δ-doped nanolayers are placed at the interface with narrow band gap material. Therefore, the electric field caused by the n-type and p-type δ-doping overcomes the quasi-electric field, and the valence band offset is minimized. As a result, an ideal band structure of the nBn detector is obtained, as shown in Fig. 2c, d. This method is beneficial for creating the required barrier layers without the problem of lattice mismatch.

3 Result and discussion

We model the InAsSb nBn detector with the δ-doped compositionally graded barrier layer, which includes contact layers, an upper-graded layer, a barrier layer, a lower-graded layer, an absorber layer, and a buffer layer. The absorber layer has a mole fraction $x_{Sb} = 0.19$ and can be grown on the InGaSb buffer layer at 150 K. This detector works based on the minority carriers, and the transfer of holes from the absorber layer to the contact layer mainly causes the dark current. As we can see from Fig. 3a, the electron density in the absorber-barrier interface region (the grading layer is considered as a part of the barrier) is depleted under significant reverse biases. The electron density decreases, leading to an increase in the SRH rate with an increasing reverse bias voltage (see Fig. 3c). Figure 3b shows that when using a large reverse bias voltage, the density of minority carriers decreases. Figure 4a depicts the current–voltage characteristic curves of the nBn structure simulated at different temperatures in the range of 125–350 K. Under − 0.2 V bias, the nBn photodetector shows a dark current of 2.596×10^{-8} A/cm^2 at 150 K. While at the $T = 300$ K, the dark current increases to 2.786×10^{-5} A/cm^2. Figure 4b shows the Arrhenius plot of dark current versus temperature reversal (1000/T) at a bias voltage of − 0.2 V. In the temperature range $T = 125$–350 K, we can see that the temperature dependency of the dark current can be nicely modeled by the equation for diffusion dominated dark current $J_{diff} \approx T^3 \exp(-E_a/(k_B T))$ and the activation energy $E_a = 0.226$ eV, which is obtained from fitting the dark current data and is almost equal to the bandgap energy of the absorber layer. The dominance of diffusion mechanism confirms the limitation due to dark current in device performance. Increase of the reverse bias voltage is associated with a decrease in the activation energy, indicating greater participation of the GR process and tunneling processes

Table 2 Recombination and defect parameters of the nBn photodetector used in the simulation

Parameter	Symbol	Value		Unit
		Absorber/contact	Compound barrier	
Electron lifetime	τ_n	0.5	1	µs
Hole lifetime	τ_p	1	1	µs
Trap energy level	E_{Trap}	$0.25E_g$	$0.5E_g$	eV
Trap concentration	N_{Trap}	1×10^9	1×10^5	cm^{-3}
SRH capture cross-section	σ_n/σ_p	5×10^{-15}	5×10^{-15}	cm^2
Electron Auger recombination coefficient	C_n	5×10^{-27}	0	cm^6·s^{-1}
Hole Auger recombination coefficient	C_p	1×10^{-27}	0	cm^6·s^{-1}
Radiative recombination coefficient	B	8.9×10^{-11}	0	cm^3·s^{-1}

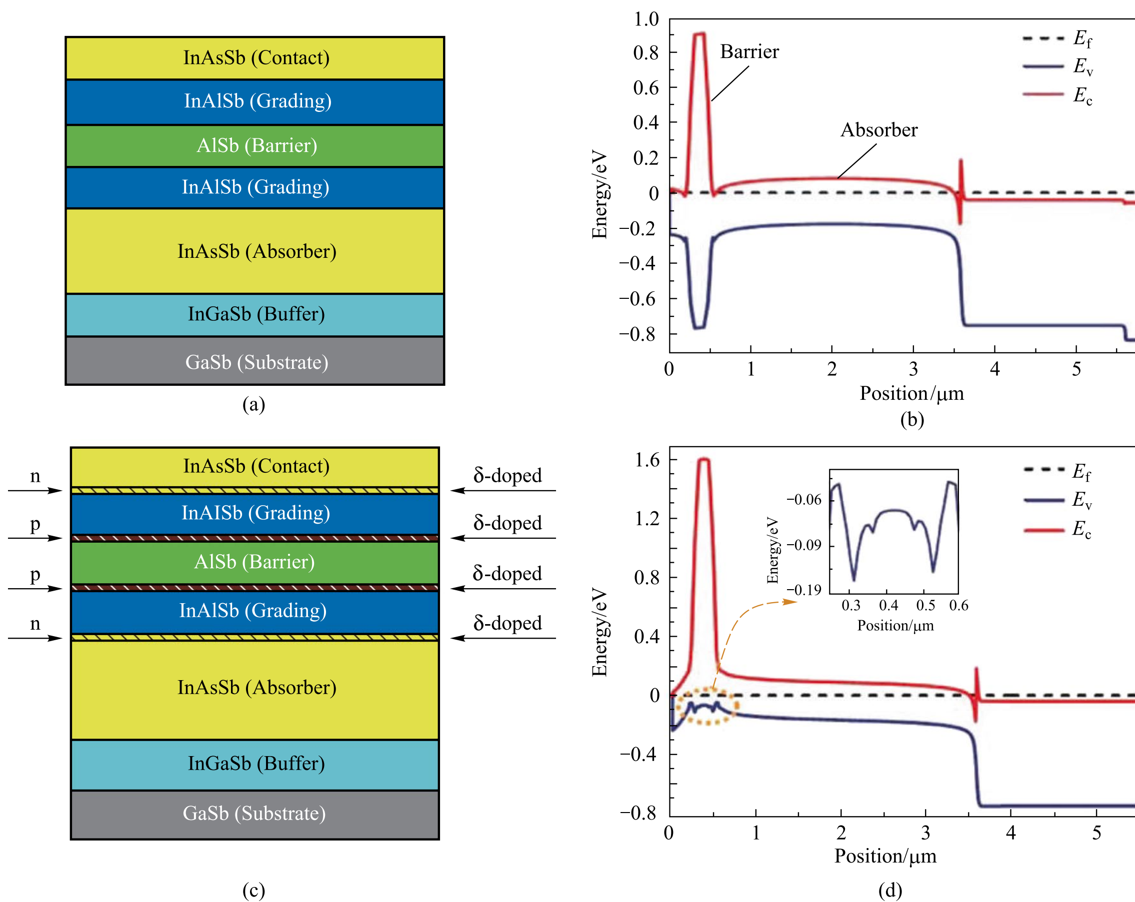

Fig. 2 InAsSb-Based nBn IR-Photodetectors; **a** Device structure and **b** energy band diagram with compositionally graded barrier (CGB) layer. **c** Device structure and **d** energy band diagram with δ-doped compositionally graded barrier (δ-DCGB) layer. The position in the vertical direction is calculated by taking the upper surface of the device as the reference

in the dark current. In the Arrhenius plot reported in Ref. [34], the authors have reported that at temperatures higher than 170 K, the dark current due to diffusion is dominant. In contrast, at temperatures lower than 170 K, the GR current is dominant, whereby the transition temperature T_0 as the transition point from GR to diffusion mechanisms is defined. It is worth mentioning that the GR current can be suppressed by the optimal design of the graded barrier of the nBn detector and the tunneling current can be prevented by choosing a thick enough barrier, and the thermionic emission current can be also suppressed by the graded design of the barrier layer.

The optical characterization results of the δ-DCGB nBn-PD device are given in Fig. 5. As can be seen, the 50% cutoff wavelength is greater than 5 μm at 150 K, which covers the wavelength range expected from the MWIR nBn detector design. In Fig. 5a, we have drawn the change of current responsivity with applied bias voltage, when the device is under various intensities of back-illumination radiations. The maximum current responsivity for a bias voltage of − 0.2 V under irradiation of 0.05 W/cm^2 is 1.6 A/W and occurs at a wavelength of 4.5 μm when the thickness of the absorber layer is 3 μm. In Fig. 5b, the current responsivity of the proposed detector in terms of wavelength is compared with the responses reported for structures reported in Refs. [35] and [36], showing the acceptable performance of the proposed photodetector.

One of the most significant criteria for evaluating the optical response of the nBn detector is the quantum efficiency (QE), which is a function of the incident radiation wavelength λ; the current responsivity R_i can be estimated from the following equation [37]:

$$\eta(\lambda) = 1.24\frac{R_\mathrm{i}}{\lambda}. \quad (5)$$

In Fig. 6a, the dependence of the quantum efficiency on the bias voltage is shown for different intensities of infrared radiations. The quantum efficiency is approximately 50% at a bias voltage of − 0.2 V, under back illumination with wavelength of 4 μm and radiation power of 0.05 W/cm^2. In Fig. 6b, we observe that the maximum quantum efficiency achieved

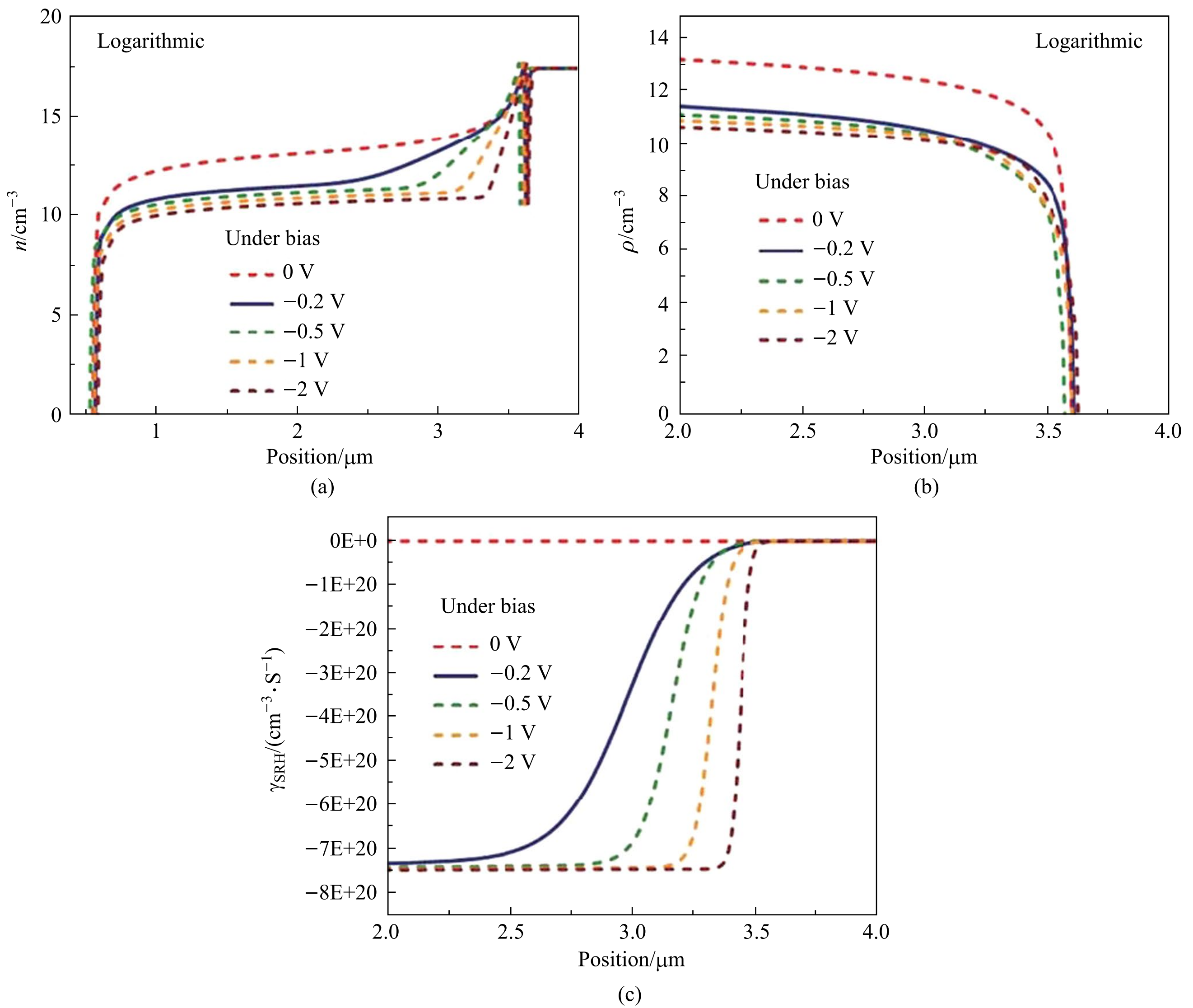

Fig. 3 Plots of the results in the absorber layer of the δ-DCGB nBn-PD device as function of the position at various applied bias voltages. **a** Electron density. **b** Hole density. **c** SRH recombination rates (negative value means generation)

at the wavelength of 4.5 μm is approximately 48.6% and the related curve is compared with those for Refs. [36, 38, 39]. The performance of nBn detectors is mainly limited by the shot noise and thermal noise in the dark current (Fig. 6c). This total noise current is the sum of the contributions from shot noise and Johnson thermal noise, and is expressed by the following equation [37]:

$$i_n(V) = \sqrt{4k_B T/RA + 2qJ_{\text{Dark}}}. \tag{6}$$

In the above noise equation, R is the dynamic resistance, T is the temperature, A is the detector area, and k_B is Boltzmann's constant. Correspondingly, specific detectivity (D^*) is calculated as an index to evaluate the signal-to-noise ratio of the detector according to the following equation [37]:

$$D^* = \frac{R_i}{i_n(V)}\sqrt{A}. \tag{7}$$

The simulation results show that for the detector structure designed with absorber doping density of 3×10^{15} cm^{-3} and a thickness of 3 μm, the noise current has the lowest value at the bias voltage of −0.2 V and is about 1.18×10^{-13} A·Hz$^{-1/2}$ (Fig. 6c).

Figure 6d shows specific detectivity, D^*, corresponding to the calculated noise current shown in Fig. 6c, revealing that at a bias voltage of − 0.2 V and intensity of 0.05 W/

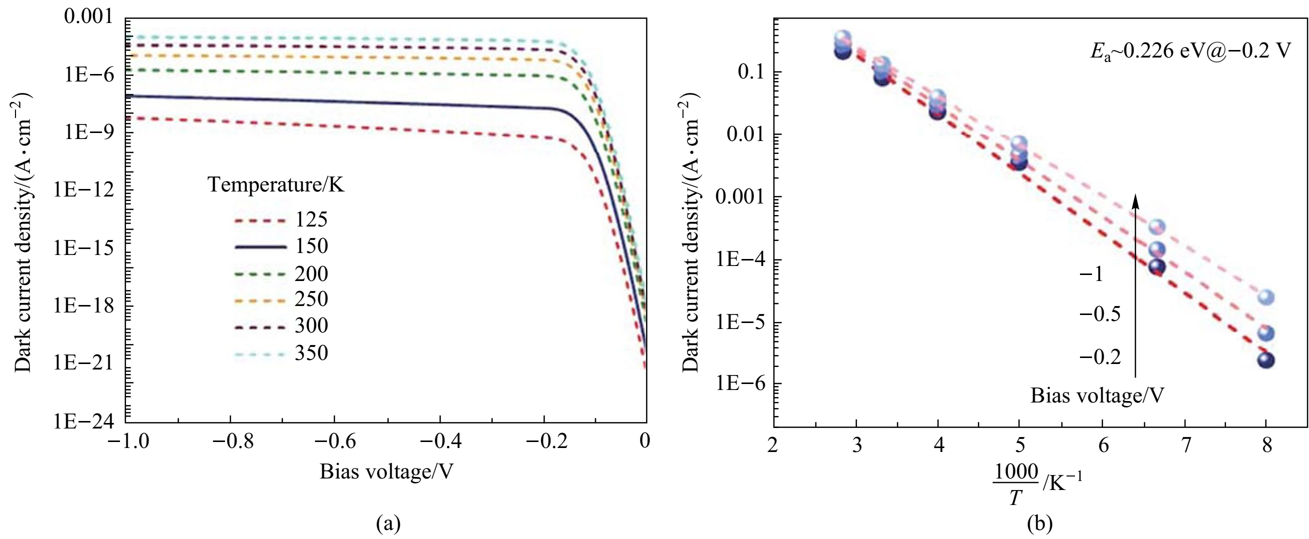

Fig. 4 Dark current of δ-DCGB nBn-PD device. **a** Dark current density vs. bias voltage. **b** Arrhenius plot of the dark current density under various applied bias voltages at temperatures from 125 to 350 K

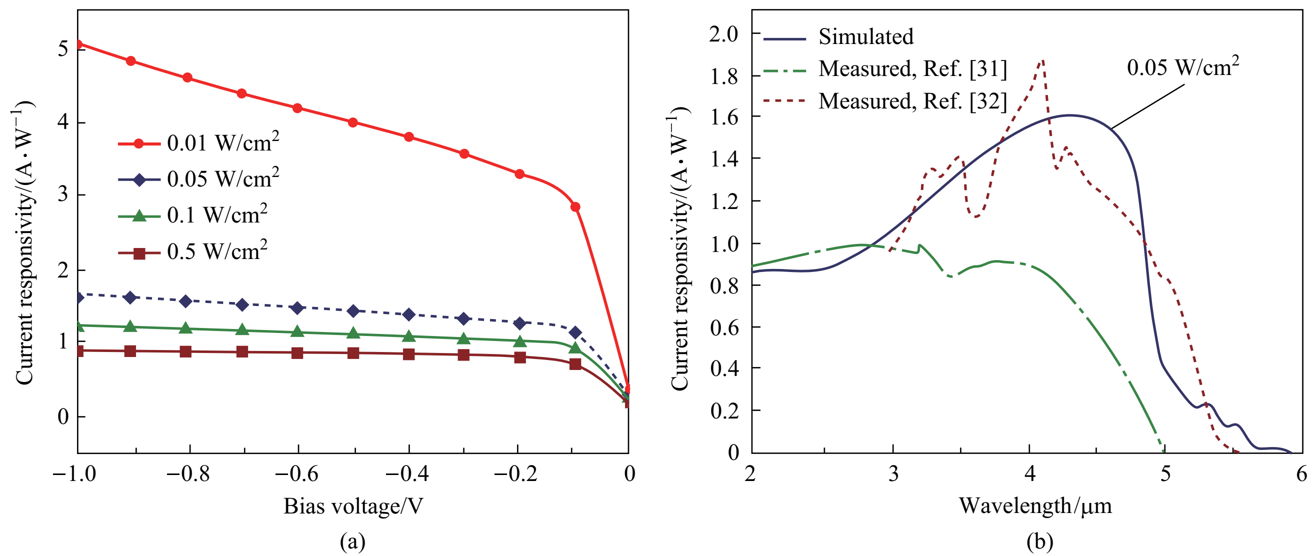

Fig. 5 Current responsivity of the δ-DCGB nBn-PD device at 150 K. **a** Responsivity versus applied bias voltages for different incident light intensities. **b** Simulated spectral response compared to the measured values

cm^2, D^* has a peak of 3.37×10^{10} cm·Hz$^{1/2}$/W. Table 3 presents the performance of the proposed photodetector and other recently reported optical detectors, showings that the proposed photodetector has comparable performance to the state-of-the-art commercial photodetectors.

The main problem in the design of optical devices is the reflection of a large part of the incident radiation on the surface of the device, so providing a solution to reduce unwanted reflections in optical systems should not be neglected. One of the solutions that can solve this problem, increasing the transmission coefficient and reducing the reflection coefficient, is the use of anti-reflective materials as a coating layer on the outer surface. The wavelength, cost, and required performance should be assessed when choosing an anti-reflection coating material for specific applications. For the MWIR range, Silicon (Si) and Germanium (Ge) materials are currently used as anti-reflection materials with high refractive indices and temperature coefficient of refractive indices (dn/dT).

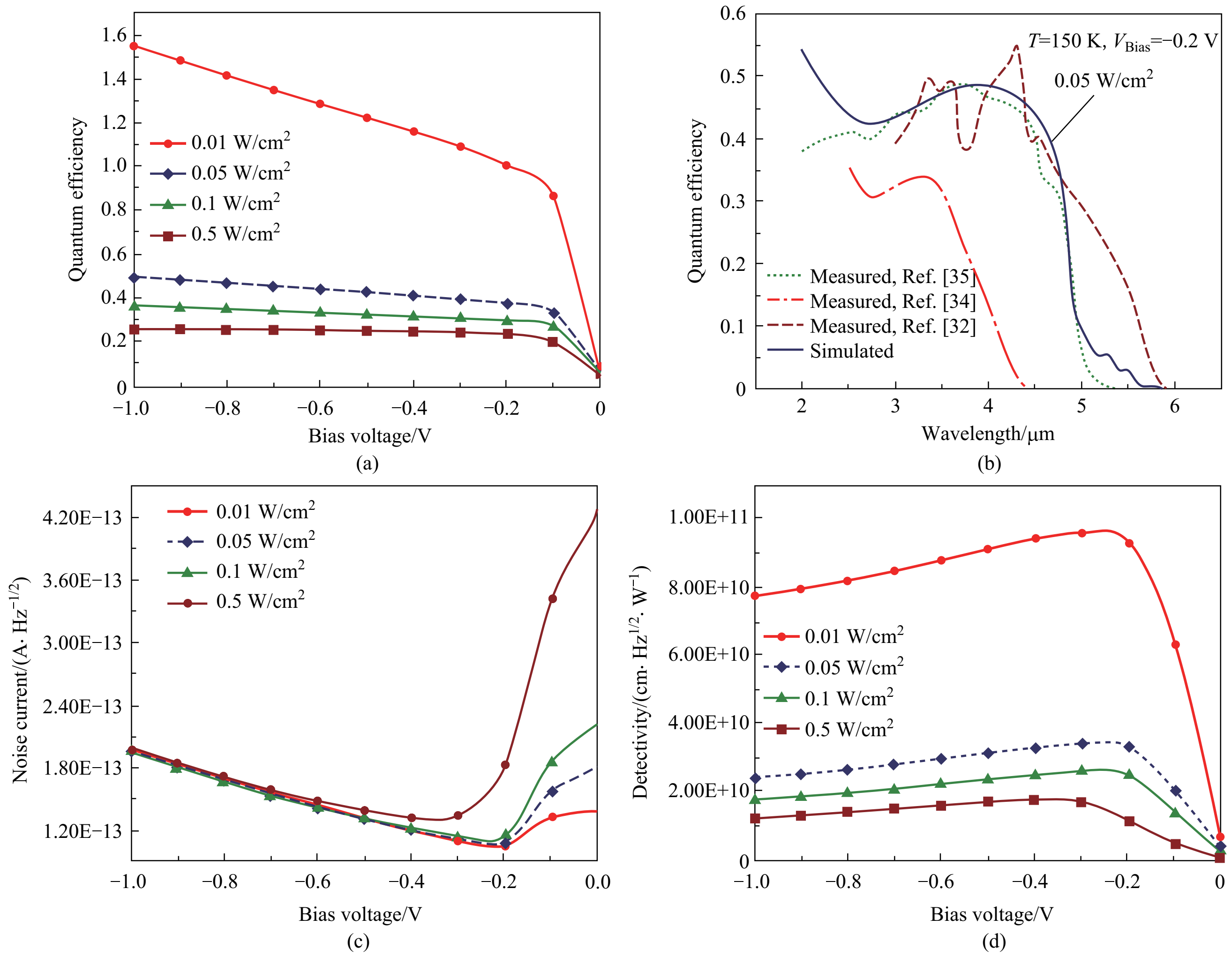

Fig. 6 Performance of the δ-DCGB nBn-PD device at 150K. **a** QE versus applied bias voltages with different intensities of infrared radiations. **b** QE versus wavelength compared to the measured values. **c** Noise current. **d** Specific detectivity versus applied bias voltages with different intensities of infrared radiations

Table 3 Summary of the performance of recently presented MWIR photodetectors

Parameters	Bulk InAsSb nBn [7]	InAs p-i-n photovoltaic [40]	$InAs/InAs_{0.6}Sb_{0.4}$ type-II superlattice (T2SL) nBn [41]	InAsSb p-i-n photovoltaic [42]	δ-DCGB InAsSb nBn (This work)
Operating temperature/K	250	300	200	300	150
Cutoff wavelength /μm	4.5	3.5	5.3	< 5	< 5
An applied bias voltage/V	− 0.2	Unbiased	0.05	− 0.5	− 0.2
Specific detectivity /($cm \cdot Hz^{1/2} \cdot W^{-1}$)	5×10^9	6.1×10^8	$\sim 10^{10}$	8.9×10^8	3.37×10^{10}

As shown in Fig. 7a, Si and Ge have a relatively lower transmittance in the MWIR range. For this reason, we used BaF_2 as an alternative MWIR anti-reflection coating material. In the simulation, we calculated the refractive index from a polynomial fitting of the refractive index data from Ref. [43](Fig. 7b). The simulation results in Fig. 7c exhibit that using a BaF_2 layer with a thickness of 0.25 μm as the anti-reflection coating layerunder the substrate., the responsivity at a bias of − 0.2 V and the radiation power of 0.05 W/cm^2 can be enhanced by about

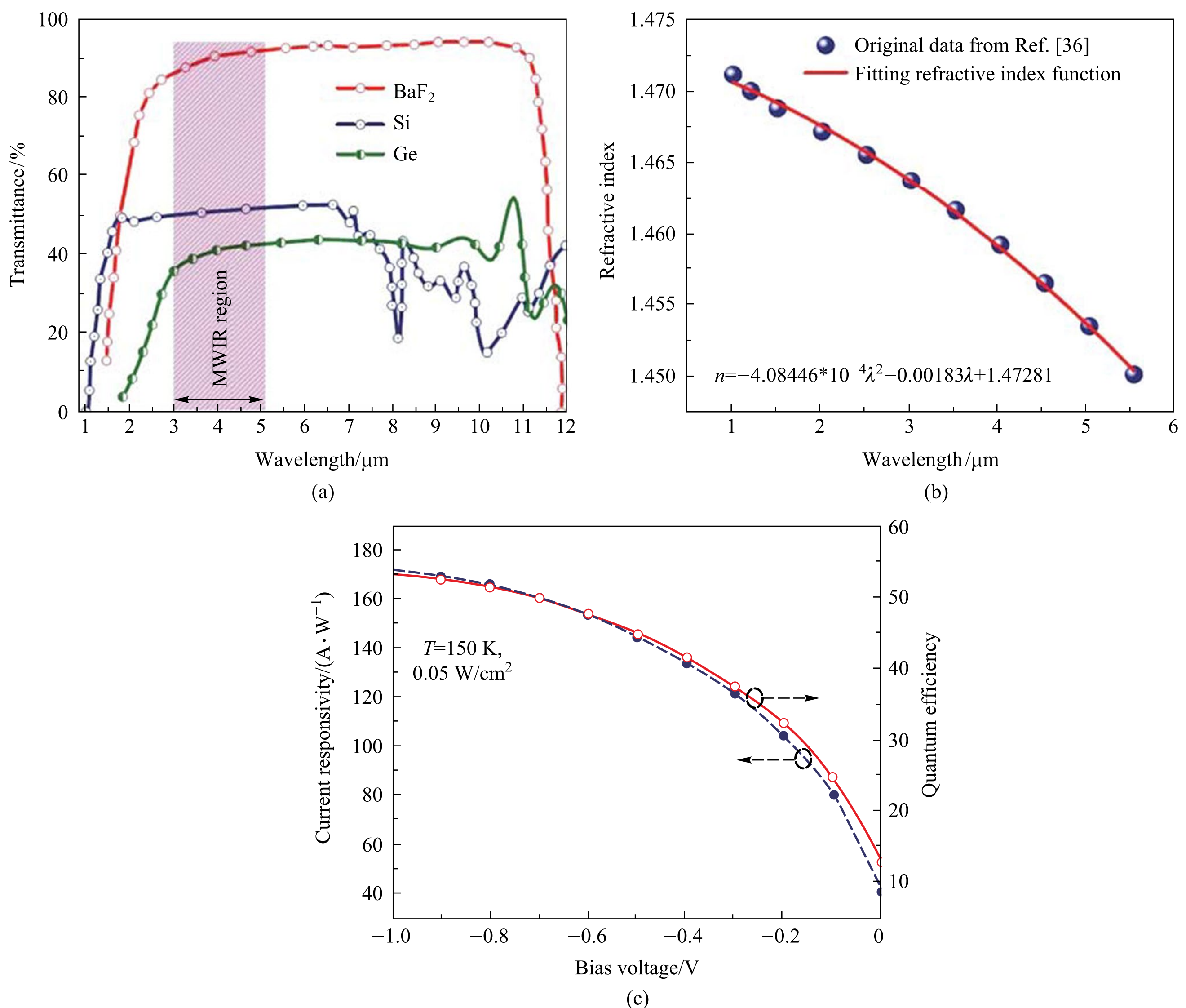

Fig. 7 δ-DCGB nBn-PD device with BaF_2 as the anti-reflection coating material at 150 K. **a** Transmittance of BaF_2 and current infrared anti-reflection coating materials. **b** Polynomial fitting of the refractive index of BaF_2. **c** Current responsivity and quantum efficiency versus the applied bias voltage.

98.5% compared to the case without anti-reflection coating layer; the quantum efficiency also increases significantly (Fig. 7c).

4 Conclusion

This work demonstrates the combination of composition grading and δ-doping as an effective band engineering method to offer an InAsSb nBn detector for high-performance MWIR applications. We used this method to reduce the valence band offset in nBn structures with $InAs_{0.81}Sb_{0.19}$ alloy absorber. Such detectors have much lower dark current than conventional detectors and significantly improved device performance can be obtained by suppressing dark current components due to SRH, BTBT, and TAT. At a temperature of 150 K, the simulation results of our proposed nBn detector have shown that the peak current responsivity at a wavelength of 4.5 μm is 1.6 A/W, and a quantum efficiency of more than 48% has been achieved. Also, the specific detectivity was about 3.37×10^{10} cm·Hz$^{1/2}$/W at 150 K with 0.05 W/cm^2 radiation and − 0.2 V bias voltage. To reduce the effects of infrared reflection from the lower surface of the nBn detector, we designed an anti-reflection coating layer of BaF_2 with a thickness of 0.5 μm under the substrate, which has

led to a better performance of the nBn detector in the simulation. This design significantly increased the responsivity and quantum efficiency of the proposed photodetector.

Author contributions All authors contributed to the study's conception and design. All authors performed data collection, simulation, and result analysis. MS wrote the first draft of the manuscript, and all authors commented on the manuscript. Both authors read and approved the final manuscript.

Availability of data and material The data that support the findings of this study are available from the corresponding author, upon reasonable request.

Declarations

Competing interests The authors declare that they have no competing interests.

Open Access This article is licensed under a Creative Commons Attribution 4.0 International License, which permits use, sharing, adaptation, distribution and reproduction in any medium or format, as long as you give appropriate credit to the original author(s) and the source, provide a link to the Creative Commons licence, and indicate if changes were made. The images or other third party material in this article are included in the article's Creative Commons licence, unless indicated otherwise in a credit line to the material. If material is not included in the article's Creative Commons licence and your intended use is not permitted by statutory regulation or exceeds the permitted use, you will need to obtain permission directly from the copyright holder. To view a copy of this licence, visit http://creativecommons.org/licenses/by/4.0/.

References

1. Rogalski, A.: $InAs_{1-x}Sb_x$ infrared detectors. Prog. Quantum Electron. **13**(3), 191–231 (1989)
2. Coderre, W.M., Woolley, J.C.: Electrical properties of $InAs_xSb_{1-x}$ alloys. Can. J. Phys. **46**(10), 1207–1214 (1968)
3. Rogalski, A.: New Ternary Alloy Systems for Infrared Detectors. In: Liquid and Solid State Crystals: Physics, Technology and Applications. 1993. SPIE (1993)
4. Rogalski, A.: Infrared Detectors 2nd ed. London—New York, CRC-Press Taylor Francis Group (2011)
5. Abautret, J., Perez, J.P., Evirgen, A., Rothman, J., Cordat, A., Christol, P.: Characterization of midwave infrared InSb avalanche photodiode. J. Appl. Phys. **117**(24), 244502 (2015)
6. Craig, A., Marshall, A.R.J., Tian, Z.B., Krishna, S., Krier, A.: Mid-infrared $InAs_{0.79}Sb_{0.21}$-based nBn photodetectors with $Al_{0.9}Ga_{0.2}As_{0.1}Sb_{0.9}$ barrier layers, and comparisons with $InAs_{0.87}Sb_{0.13}$ pin diodes, both grown on GaAs using interfacial misfit arrays. Appl. Phys. Lett. **103**(25), 253502 (2013)
7. Soibel, A., Hill, C.J., Keo, S.A., Hoglund, L., Rosenberg, R., Kowalczyk, R., Khoshakhlagh, A., Fisher, A., Ting, D.Z.Y., Gunapala, S.D.: Room temperature performance of mid-wavelength infrared InAsSb nBn detectors. Appl. Phys. Lett. **105**(2), 023512 (2014)
8. Klipstein. P., Gross. Y., Aronov. D., Ezra M. ben, Berkowicz, E, Cohen. Y., Fraenkel. R., Glozman. A., Grossman. S., Klin. O., Lukomsky. I., Marlowitz. T., Shkedy. L., Shtrichman. I., Snapi. N., Tuito. A., Yassen. M., Weiss. E.: Low SWaP MWIR detector based on XBn focal plane array. In: Proceedings of Infrared Technology and Applications XXXIX. SPIE (2013)
9. Klipstein, P.: XBnn and XBpp infrared detectors. J. Cryst. Growth **425**, 351–356 (2015)
10. Klipstein, P., Avnon, E., Benny, Y., Berkowicz, E., Cohen, Y., Dobromislin, R., Fraenkel, R., Gershon, G., Glozman, A., Hojman, E., Ilan, E., Karni, Y., Klin, O., Kodriano, Y., Krasovitsky, L., Langof, L., Lukomsky, I., Nevo, I., Nitzani, M., Pivnik, I., Rappaport, N., Rosenberg, O., Shtrichman, I., Shkedy, L., Snapi, N., Talmor, R., Tessler, R., Weiss, E., Tuito, A.: Development and production of array barrier detectors at SCD. J. Electron. Mater. **46**(9), 5386–5393 (2017)
11. Shkedy. L, Brumer. M, Klipstein. P, Nitzani. M, Avnon. E, Kodriano. Y, Lukomsky. I, Shtrichman. I.: Development of 10 μm pitch XBn detector for low SWaP MWIR applications. In: Proceedings of Infrared Technology and Applications XLII. SPIE (2016)
12. Rhiger, D.R., Smith, E.P., Kolasa, B.P., Kim, J.K., Klem, J.F., Hawkins, S.D.: Analysis of III–V superlattice nBn device characteristics. J. Electron. Mater. **45**(9), 4646–4653 (2016)
13. Klipstein, P., Benny, Y., Cohen, Y., Fraenkel, N., Gliksman, S., Glozman, A., Hadari, N., Hirsh, I., Katz, M., Klin, O., Langof, L., Lukomsky, I., Marderfeld, I., Nitzani, M., Rakhmilevich, D., Shusterman, S., Shafir, I., Shtrichman, I., Sicron, N., Snapi, N., Yaron, N.: XBn and XBp detectors based on type II superlattices. J. Electron. Mater. **51**(9), 1–6 (2022)
14. Maimon, S., Wicks, G.: nBn detector, an infrared detector with reduced dark current and higher operating temperature. Appl. Phys. Lett. **89**(15), 151109 (2006)
15. Wicks, G.,Savich. G. R., Pedrazzani. J. R., Maimon. S.: Infrared detector epitaxial designs for suppression of surface leakage current. In: Proceedings of Quantum Sensing and Nanophotonic Devices VII. SPIE (2010)
16. Savich, G., Pedrazzani, J.R., Sidor, D.E., Maimon, S., Wicks, G.W.: Dark current filtering in unipolar barrier infrared detectors. Appl. Phys. Lett. **99**(12), 121112 (2011)
17. Ting, D.Z., Soibel, A., Khoshakhlagh, A., Gunapala, S.D.: Theoretical analysis of nBn infrared photodetectors. Opt. Eng. **56**(9), 091606 (2017)
18. Akhavan, N., Umana-Membreno, G.A., Jolley, G., Antoszewski, J., Faraone, L.: A method of removing the valence band discontinuity in HgCdTe-based nBn detectors. Appl. Phys. Lett. **105**(12), 121110 (2014)
19. Akhavan, N.D., Umana-Membreno, G.A., Gu, R., Asadnia, M., Antoszewski, J., Faraone, L.: Superlattice barrier HgCdTe nBn infrared photodetectors: validation of the effective mass approximation. IEEE Trans. Electron Dev. **63**(12), 4811–4818 (2016)
20. Deng, G., Yang, W., Zhao, P., Zhang, Y.: High operating temperature InAsSb-based mid-infrared focal plane array with a band-aligned compound barrier. Appl. Phys. Lett. **116**(3), 031104 (2020)
21. Deng, G., Yang, W., Gong, X., Zhang, Y.: High-performance uncooled InAsSb-based pCBn mid-infrared photodetectors. Infrared Phys. Technol. **105**, 103260 (2020)
22. Konovalov, G. G., Mikhailova. M. P., Andreev. I. A., Moiseev. K. D., Ivanov. E. V., Mikhailov. M. Y., Yakovlev. Y. P.: Photovoltaic detector based on type II heterostructure with deep AlSb/InAsSb/AlSb quantum well in the active region for the mid-infrared spectral range. In: Proceedings of Journal of Physics: Conference Series. IOP Publishing (2013)
23. Uzgur, F., Karaca, U., Kizilkan, E., Kocaman, S.: All InGaAs unipolar barrier infrared detectors. IEEE Trans. Electron Dev. **65**(4), 1397–1403 (2018)
24. Akhavan, N.D., Umana-Membreno, G.A., Gu, R., Antoszewski, J., Faraone, L.: Delta doping in HgCdTe-based unipolar barrier photodetectors. IEEE Trans. Electron Dev. **65**(10), 4340–4345 (2018)

25. Rogalski, A., Ciupa, R., Larkowski, W.: Near room-temperature InAsSb photodiodes: theoretical predictions and experimental data. Solid-State Electron. **39**(11), 1593–1600 (1996)
26. Rogalski, A.: New Ternary alloy systems for infrared detectors. In: Proceedings of Liquid and Solid State Crystals: Physics, Technology and Applications. SPIE Press (1994)
27. Madelung, O.: Physical Data. In: Semiconductors—Basic Data. p. 5–298. Berlin, Springer (1996)
28. Vurgaftman, I., Meyer, J., Ram-Mohan, L.: Band parameters for III–V compound semiconductors and their alloys. J. Appl. Phys. **89**(11), 5815–5875 (2001)
29. D'souza, A., Robinson, E., Ionescu, A.C., Okerlund, D., de Lyon, T.J., Sharifi, H., Roebuck, M., Yap, D., Rajavel, R.D., Dhar, N., Wijewarnasuriya, P.S., Grein, C.: Electrooptical characterization of MWIR InAsSb detectors. J. Electron. Mater. **41**(10), 2671–2678 (2012)
30. Kabanau, D., Lebiadok, Y., Yakovlev, Y.P.: Auger recombination and amplified luminescence in InAsSb/InAsSbP Leds at 10–60 K. J. Appl. Spectrosc. **84**(5), 843–849 (2017)
31. Chen, G., Sun, W., Lv, Y.: Empirical expression for the composition and temperature dependence of the energy gap in InAlSb. Infrared Phys. Technol. **81**, 262–265 (2017)
32. Rogalski, A., Orman, Z.: Band-to-band recombination in $InAs_{1-x}Sb_x$. Infrared Phys. **25**(3), 551–560 (1985)
33. Martyniuk, P., Rogalski, A.: Modeling of InAsSb/AlAsSb nBn HOT detector's performance limit. In: Proceedings of Infrared Technology and Applications XXXIX. SPIE (2013)
34. Deng, G., Chen, D., Yang, S., Yang, C., Yuan, J., Yang, W., Zhang, Y.: High operating temperature pBn barrier mid-wavelength infrared photodetectors and focal plane array based on InAs/InAsSb strained layer superlattices. Opt. Express **28**(12), 17611–17619 (2020)
35. Kulikov, V., Maslov, D.V., Sabirov, A.R., Solodkov, A.A., Dudin, A.L., Katsavets, N.I., Kogan, I.V., Shukov, I.V., Chaly, V.P.: nBn-photodiode based on InAsSb/AlAsSb alloys with a long-wavelength cutoff of 5 μm. Semiconductors **52**(13), 1743–1747 (2018)
36. Chen, D., Li, D., Xiao, T., Shi, J., He, Y., Gong, X., Yang, S., Yue, B., Zhao, J., Yang, W., Deng, G.: Bulk InAsSb-based upside-down pCBn photodetectors with greater than 5 μm cut-off wavelength. AIP Adv. **12**(5), 055327 (2022)
37. Martyniuk, P., Rogalski, A.: Performance limits of the mid-wave InAsSb/AlAsSb nBn HOT infrared detector. Opt. Quantum Electron. **46**(4), 581–591 (2014)
38. Nolde, J.A., Jackson, E.M., Kim, M., Kim, C.S., Canedy, C.L., Warren, M.V., Tomasulo, S., Affouda, C.A., Cleveland, E.R., Vurgaftman, I., Meyer, J.R., Aifer, E.H.: Temperature dependence of quantum efficiency enhancement using plasmonic gratings on nBn detectors with thin absorbers. J. Nanophotonics **13**(4), 046007 (2019)
39. Soibel. A., Ting. D. Z., Hill. C. J., Fisher. A. M, Hoglund. L, Keo. S. A., Gunapala. S. D.: Extended cut-off wavelength nBn detector utilizing InAsSb/InSb digital alloy absorber. In: Proceedings of Quantum Sensing and Nano Electronics and Photonics XIV. SPIE (2017)
40. Khai, L.W., Hua, T.K., Daosheng, L., Wicaksono, S., Fatt, Y.S.: Room temperature 3.5 μm mid-infrared InAs photovoltaic detector on a Si substrate. IEEE Photonics Technol. Lett. **28**(15), 1653–1656 (2016)
41. Martyniuk, P., Michalczewski, K., Tsai, T.Y., Wu, C.H., Wu, Y.R.: A thermoelectrically cooled nBn type-II superlattices InAs/InAsSb/B-AlAsSb mid-wave infrared detector. Phys. Status Solidi A **217**(6), 1900522 (2020)
42. Tong, J., Tobing, L.Y.M., Qian, L., Suo, F., Zhang, D.H.: $InAs_{0.9}Sb_{0.1}$-based hetero-pin structure grown on GaSb with high mid-infrared photodetection performance at room temperature. J. Mater. Sci. **53**(18), 13010–13017 (2018)
43. Leviton, D.B., Frey, B.J., Kvamme, T.: High accuracy, absolute, cryogenic, refractive index measurements of infrared lens materials for JWST NIRCam using CHARMS. In: Proceedings of Cryogenic Optical Systems and Instruments XI. SPIE (2005)

Maryam Shaveisi received a B.Sc. degree in Communication Engineering and an M.Sc. degree in Nano/Microelectronic Device Engineering from the Kermanshah University of Technology (KUT), Kermanshah, Iran, in 2016 and 2018, respectively. She is currently a Ph.D. research assistant at the Aerospace Research Institute (Ministry of Science, Research and Technology), Tehran, Iran. Her research interests include designing low-power quantum-based devices, design and fabrication devices based on III-V compound semiconductors, IR-photodetectors, Infrared absorber and anti-reflective coating layers, sensors, biosensors, and all related electronic devices.

Peiman Aliparast received an M.Sc. degree from Urmia University, Urmia, Iran, in 2007 and a Ph.D. degree from the University of Tabriz, Tabriz, Iran, in 2012 both in Electronics Engineering. From 2004 to 2008, he was with the Microelectronics Research Laboratory at Urmia University, Urmia, Iran, and from 2008 to 2012, he was a research assistant at the Integrated Circuits Research Laboratory, University of Tabriz, Tabriz, Iran. He is currently an assistant professor and director of Microsystems Lab in Aerospace Research Institute (Ministry of Science, Research and Technology), Tehran, Iran. He has joined the AIC Lab at the University of Pavia, Italy, as a visiting research fellow, where he has been enveloped in millimeter-wave integrated circuit projects. His research interests are smart optical image sensors for biomedical applications and high-frequency integrated circuits for telecommunication systems. He is a member of the Iran Microelectronics Association (IMA).